JOURNAL OF MATERIALS SCIENCE 33 (1998) 1619–1625

# Inelastic response of confined aluminium oxide under dynamic loading conditions

J. LANKFORD, C. E. ANDERSON Jr, A.J. NAGY, J. D. WALKER, A. E. NICHOLLS, R. A. PAGE
*Southwest Research Institute, Materials and Structures Division, San Antonio, TX 78238, USA*

Previous efforts to explore the compressive strength of ceramics as a function of confining pressure at high strain rates have been limited by the maximum hydrostatic pressure that could be achieved within the experimental apparatus. An alternate procedure, using an autofrettaged confinement ring, has been designed to achieve higher confining pressures. A 6.2 GPa stress pulse, of approximately 20 μs duration, was used to load a 99.5% pure cylindrical aluminium oxide specimen under a hydrostatic load of approximately 650 MPa. The specimen remained intact and showed no evidence of fracture under scanning electron microscopy (SEM). Transmission electron microscopy (TEM), however, showed extensive evidence of plastic flow; the microcracks that were observed were associated with dislocation arrays. Static and dynamic yield strengths as a function of strain rate are compared. 

## 1. Introduction

A number of investigators have demonstrated that confinement can have a major effect on the strength of brittle materials; this has been shown for both rocks and ceramics, e.g. [1, 2]. In particular, compressive failure strength generally increases significantly with confining pressure, a dependence that can be interpreted to establish empirically the relevant failure criterion (e.g. Mohr–Coulomb, Drucker–Prager) for a given material. It is known that the effect of pressure is manifested physically in the closure of axial microcraks, the coalescence of which ultimately causes compressively loaded specimens to fail. Failed material in powder form also is strengthened by confinement, although the strength of this state at a given confining pressure is much reduced in comparison with unfailed ceramic bodies. In this (powder) case, increasing pressure also raises the slope of the stress–strain curve, while for solid material, the elastic modulus is essentially pressure-insensitive.

Research on brittle materials in which both confining pressure and strain rate were varied in combination was, until recently, limited to rocks [1, 3–4]. However, because the superposition of confinement and high strain rate occurs during the ballistic penetration of ceramics, studies have been initiated to examine these effects in ceramics [5, 6]. The experiments described previously [5] were performed using a split-Hopkinson pressure bar (SHPB) apparatus [7]; for tests with radial confining pressure $P_A$, a special pressure vessel was utilized. In these experiments, the hydrostatic pressure was first raised to the desired level by pumping fluid into the pressure vessel while a servo-controller matched the axial stress to the pressure. Then the axial load was increased under displacement control at fixed pressure. The value of the strain rate, $\dot{\varepsilon}$, was determined by measuring the stress rate, $\dot{\sigma}$, and calculating $\dot{\varepsilon}$ using the appropriate value for Young's modulus for each material, i.e. $\dot{\varepsilon} = \dot{\sigma}/E$ [8]. Solid ceramic specimens were loaded by means of tapered alumina platens. Specimens were sealed within thin, heat-shrinkable Teflon tubing, overlapping the small ends of the platens in order to prevent the silicon-based pressure fluid from infiltrating surface pores and causing premature failure. Similarly, powdered compression specimens were produced by tamping the ball-milled fines into heat-shrinkable tubing that had been shrunk to fit snugly over alumina platens. These specimens, like the solid ceramics, were 6.4 mm diameter by 12–13 mm long. Anderson *et al.* [7] used numerical simulations to explore, evaluate, and substantiate the assumptions and interpretation of the experimental data.

In this earlier work [5], considerably different behaviour was observed for SiC and Pyroceram under confinement. For SiC, Fig. 1, the $\sigma_z$ versus time curve for $P_A = 0$ is roughly symmetric, suggesting that the specimen failed in a normal brittle fashion. However, with increasing pressure, the curve becomes quite asymmetric, as is especially noticeable for $P_A = 200$ MPa. The specimen did not fracture at 320 MPa confining pressure. On the other hand, the post-failure behaviour of Pyroceram, Fig. 2, is more complex than that of SiC. It resembles very much, in fact, the phenomenon observed by Heard and Cline [8] for BeO and AlN subject to compression under confining pressure at strain rates on the order of $5 \times 10^{-5}\,s^{-1}$. In their work, it was hypothesized that

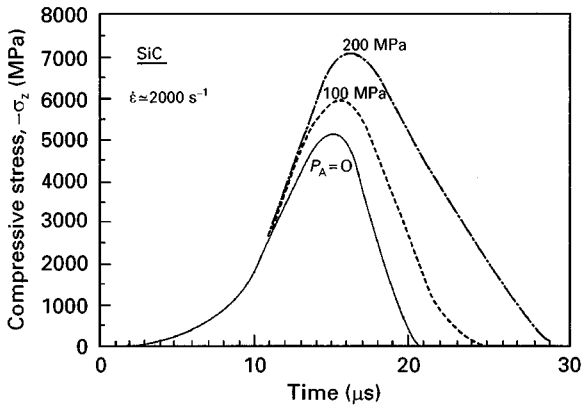


*Figure 1* Compressive strength versus time for SiC at various confining pressures.

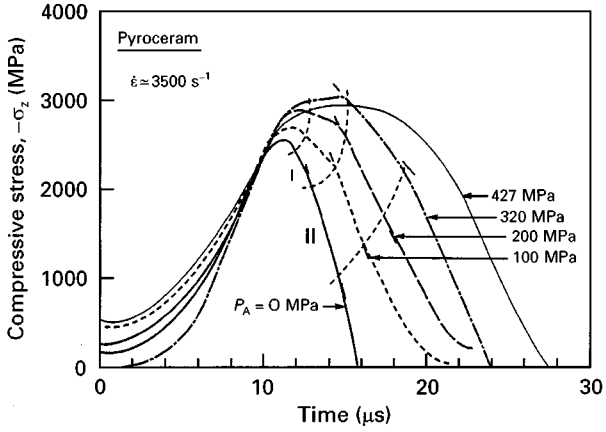


*Figure 2* Compressive strength versus time for Pyroceram at various confining pressures.

the softening-to-hardening trend with rising pressure was caused by a brittle-to-ductile transformation, i.e. pressure above a critical level suppressed fracture and permitted plastic flow via dislocation motion. It is interesting to note that Heard and Cline saw no such pressure-induced plastic flow for $Al_2O_3$ subject to confinement at pressures as high as 1.25 GPa; i.e. it failed in an apparently brittle fashion at this and lower pressures.

However, there are several limitations to the experimental methodology of the previous work [5]. First, the maximum confining pressure was, in practice, limited to approximately 320 MPa (427 MPa was achieved for only a couple of tests, e.g. Fig. 2). At higher pressures, the seals did not contain the hydraulic fluid. Additionally, there were safety concerns relative to the high static prestress and the linearity of the SHPB system (small deviations from linearity increased the likelihood of buckling of either the transmitter or receiver bar). To overcome these limitations, a different procedure to provide the confining pressure was needed. Chen and Ravichandran [9] have recently shown that lateral confinement can be applied by shrink fitting a metal sleeve on to the lateral surface of a cylindrical ceramic specimen. Using this approach, they report that lateral confinement pressures as high as 200 MPa were developed for aluminium nitride, which was then subjected to moderate dynamic strain rates ($500\,s^{-1}$) using a split-Hopkinson pressure bar. Under these conditions, samples were observed to fail by microfracture coalescence over a loading period of more than 300 μs.

The present effort describes a modification of this approach to achieve higher confining pressures, higher strain rates, and shorter loading periods (about 10 μs). Also, whereas the approach of Chen and Ravichandran leads to an indeterminate stress state within the specimen, the present approach puts the specimen under a well-defined state of pure hydrostatic pressure. It will be shown that the sample does not fail under the latter conditions, and that extensive plastic flow is introduced.

## 2. Experimental procedure

### 2.1. Autofrettage concept

To achieve higher pressures, a steel confinement ring is shrink-fitted around the ceramic specimen. To maintain an elastic response in the confinement ring, the ring is actually composed of two concentric rings, with the outer ring shrink-fitted to the inner. This autofrettaged assembly is then shrink-fitted to the ceramic specimen, producing a compressive stress state in the specimen. During the shrink fitting, the ceramic is compressively loaded in order to achieve an overall hydrostatic state of stress. The Appendix provides an analytical theory for determining the subsequent pressure on the ceramic specimen.

The autofrettage device was constructed from two concentric steel rings. Letting $a$ be the radius of the specimen, the concentric steel rings had outer diameters of approximately $b = 2a$ and $c = 5a$, respectively, which were arrived at by examining the analytical solution; $c$ is large enough for the outer ring to appear to have nearly infinite extent (which leads to higher pressures). In the actual apparatus, a high strength steel (yield strength approximately 2.4 GPa) was used in fabricating the autofrettage sleeve. The design is such that the maximum confining stress is actually limited by the temperature to which the autofrettaged ring can be raised, because for a wide range of temperatures the response is elastic.

Dimensions of the test specimen are tailored to provide the appropriate fit with the sleeve. Assuming a "perfect fit" for the specimen at a sleeve temperature of 410 °C (the actual temperature used in assembly was, of course, higher to allow clearance), and a specimen diameter of 0.6332 cm (the diameter of the specimen used in the autofrettage experiment), the hydrostatic confining pressure after completion of the test fixture assembly is 650 MPa. Small changes in the magnitude of interference have a pronounced effect on the amplitude of the generated confining pressure. A 0.000 254 cm change will increase or decrease the confining pressure by roughly 60 MPa. Using higher temperatures for the "perfect fit" (and increasing the specimen diameter accordingly) produces higher pressures: for example, 538 °C gives 930 MPa.

To perform the confining pressurization procedure and the subsequent high strain-rate loading of the specimen, an experimental apparatus was designed

and fabricated [10, 11]. The purpose of the apparatus is three-fold:

1. to support the specimen and the "confining chamber" components, comprised of the confining sleeve and the loading anvils, during the autofrettaging procedure;
2. to provide the necessary alignment and guidance of the components during the autofrettaging assembly process; and
3. to act as a reaction frame for the application and maintenance of the axial component of the hydrostatic pressure.

During the autofrettaging procedure, the confining sleeve is held in its proper position by a brass support sleeve, while the lower loading anvil is supported by the instrumented reaction bar. In addition to its supporting function, the support sleeve serves as a shield for the reaction bar, protecting the bar from direct heating by the induction coil. To provide further protection for the strain gauges, the reaction bar is also equipped with two water-cooled pads to mitigate the effect of the heat conducted into the bar from the lower loading anvil during the autofrettaging procedure.

Once proper alignment is established, the autofrettaging procedure is performed in a servo-controlled hydraulic test system under closed-loop load control, where the output signal from the strain gauge on the reaction bar is used as the feedback. The confining sleeve is inductively heated to 510–525 °C as rapidly as possible. Upon reaching this temperature, the shield, located between the specimen and the confining ring, is removed and an appropriate axial load, proportional to the predicted confining pressure, is applied to the transmitter bar with the system. Application of the load results in the insertion of the specimen into the confining ring, and the specimen bottoms out on the lower loading anvil. The applied axial load is maintained throughout the cooling sequence. Pre-application of the axial pressure is permissible as long as the applied stress is less than the compressive yield strength of the specimen.

After the confining system reaches room temperature, the hydraulic actuator of the autofrettaged system is lowered into its final axial placement and rotated into its locking position. While maintaining axial load control with the hydraulic test system, the actuator of the autofrettaging apparatus is pressurized until it takes over the axial load from the test system. At this point, the system is switched to position control mode, and the output signal from the reaction bar is switched to controlling the axial stress with the actuator of the autofrettaged system. While maintaining the proper axial stress, the apparatus is transferred to a pre-aligned cradle on the SHPB system for high-strain-rate loading of the specimen.

## 2.2. Testing procedures

A 0.6332 cm diameter by 1.27 cm long cylindrical specimen was prepared and inserted within the autofrettage device as outlined in the previous section. The specimen was 99.5% pure $Al_2O_3$ (Coors AD 995, Golden, CO), with a density of 3.90 g cm$^{-3}$.

The transition loading platens were machined from tungsten carbide. Confined high-strain-rate experiments were performed using the hybrid SHPB consisting of strain-gauged, 0.154 m long incident bar and a similarly gauged transmitter bar only 0.077 m in length. A short (0.05 m), high-strength steel projectile was fired at 66 m s$^{-1}$ to generate a 20 μs stress pulse within the bar system. Because the platens reduce the load-carrying cross-sectional area by a factor of four, the specimen sees approximately a 6.2 GPa stress pulse.

The apparatus was examined after the test. The tungsten carbide platens were shattered; no damage was visible to the confined $Al_2O_3$. It was decided to sacrifice the autofrettage assembly to examine the ceramic further. This is discussed below.

Previous work in our laboratory has shown [12] that stress-rate signals derived from the transmitter bar are compromised by dispersion phenomena for specimen strain rates above about 2700 s$^{-1}$, an effect that was recently modelled and rationalized by Ravichandran and Subhash [13]. Accordingly, a series of experiments was performed involving the placement of strain gauges at various locations along the transmitter bar to provide an empirical relationship that can be used to correct transmitter bar data and bring it into agreement with that obtained by specimen-mounted gauges. Because the confinement process obviously precluded the latter, corrected transmitter bar data were utilized to derive the stress–time history of the sample.

Tests also were run with no confinement at strain rates of $1.5 \times 10^{-4}$ s$^{-1}$ and 2066 s$^{-1}$, the former using a servo-controlled hydraulic load machine and the latter the SHPB. In these cases, the samples were strain-gauged to permit determination of the stress–strain behaviour.

Following testing under confinement, the entire autofrettage device was sectioned using a diamond saw; half of the sample was polished and examined by scanning electron microscopy (SEM). From the other half, transmission electron microscope specimens were sectioned, cored, and ion-milled. Similar transmission electron microscopy (TEM) specimens were obtained from untested alumina. Both groups of samples were examined in a 200 keV transmission electron microscope.

## 3. Results

Under unconfined conditions, specimens behave similarly regardless of loading rate, i.e. loading is linear elastic to failure, which was marked by catastrophic rubbling of the sample. For quasistatic loading ($\dot{\varepsilon} = 1.5 \times 10^{-4}$ s$^{-1}$) the compressive strength was 2472 MPa, while under dynamic deformation ($\dot{\varepsilon} = 2066$ s$^{-1}$), the strength rose to 3262 MPa.

Shown in Fig. 3 is the time history of the stress pulse experienced by aluminium oxide confined within the autofrettage device and tested in the SHPB. The strain rate leading up to the peak stress (transmitter bar signal corrected for dispersion) was 5940 s$^{-1}$. Immediately upon reaching the maximum stress amplitude

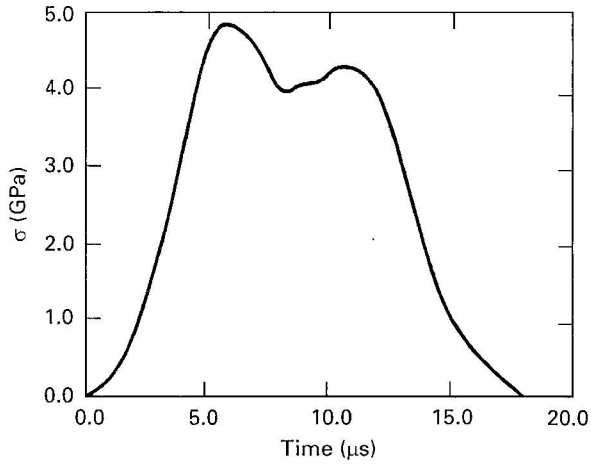


*Figure 3* Stress–time history within a confined $Al_2O_3$ sample, sharing load drop followed by stable hardening.

(beyond the hydrostat) of 4.85 GPa, the stress falls slightly and the sample immediately begins to undergo apparent stable plastic flow with hardening. This lasts for a period of about 3.5 μs, so that the sample experienced high stresses ( >4 GPa) for approximately 8 μs. The incident pulse length of ~20 μs was not realized within the sample due to failure of the platens, although the specimen itself survived. When the autofrettage device was sectioned, the sample was revealed to be essentially intact, with the exception of a single large crack transverse to the applied axial load. This clearly was not a compressive failure, but rather an incidental fracture due to a dynamic post-test tensile release wave, or to relaxation induced by the sectioning itself.

Under the SEM, no evidence of microfracture was visible on polished sections taken from the confined high-strain-rate specimen. Transmission electron microscopy (TEM), however, showed extensive evidence of plastic flow. Numerous grain-boundary dislocation pile-ups (arrows, Figs 4–7) were observed, as well as deformation on multiple slip systems (Fig. 6). Some of the pile-ups induced dislocation activity in adjacent grains (Fig. 4), while others nucleated small transgranular microcracks (arrows, Figs 5–7). It should be noted that no microcracks were observed except in association with dislocation arrays, and no large (multi-grain) cracks were observed at all.

## 4. Discussion

It is well known [8, 14] that in the absence of confinement, alumina (like other brittle ceramics) fails in compression via the nucleation growth and coalescence of (roughly) axially oriented microcracks. This is an apparently brittle fracture process, and usually occurs at stress levels below those characteristic of shock-loading conditions, where compressive "failure" is represented by the Hugoniot elastic limit (HEL). The latter is the axial stress at which the material, loaded in compression under uniaxial strain constraint (perfect confinement), can no longer support purely elastic strain and begins to flow through either plastic flow or cataclastic (flow-like) fracture processes

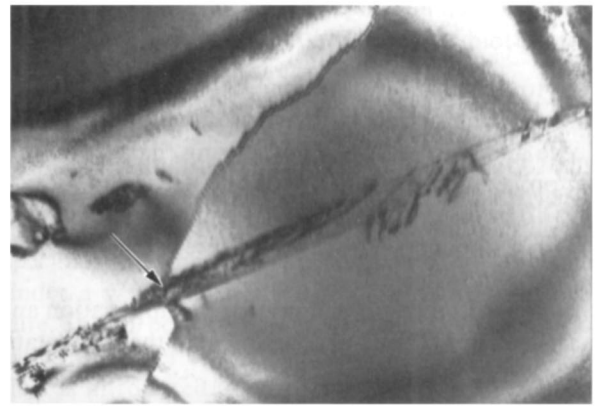

*Figure 4* Slip-band pile-up at GB (arrow), nucleating a slip band in an adjacent (left) grain.

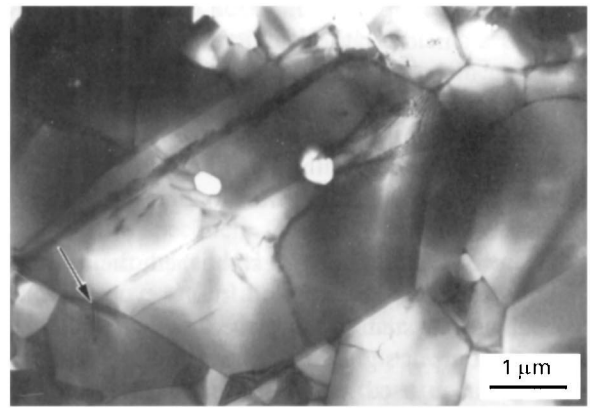


*Figure 5* Slip-band pile-up at GB (arrow), nucleating a transgranular microcrack in adjacent grains. Nearby are slip bands that have caused no microfracture.

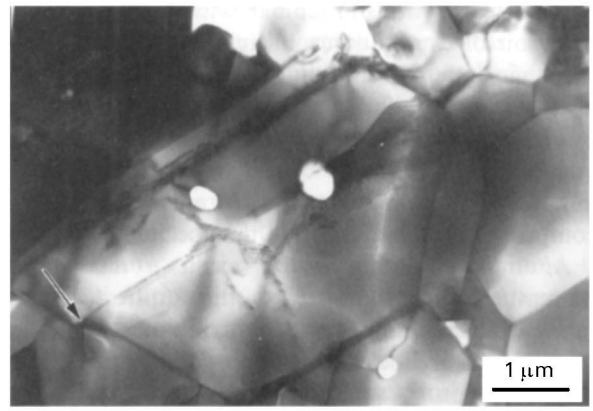


*Figure 6* Tilted view of image shown in Fig. 4, showing multiple slip-system dislocation activity.

[15]. Contrasting with the (latter) high strain-rate situation, in which confinement is generated by inertial effects, is microhardness indentation under quasistatic conditions, with confinement provided by the indentor and elastic surround. In this case, the hardness, $H$, is a measure of compressive yielding, always at pressures much in excess of the unconfined compressive strength, $\sigma_c$.

Measured values of $H$ and HEL thus include confinement terms superimposed on the uniaxial intrinsic static and dynamic yield strengths, $Y_S$ and $Y_D$.

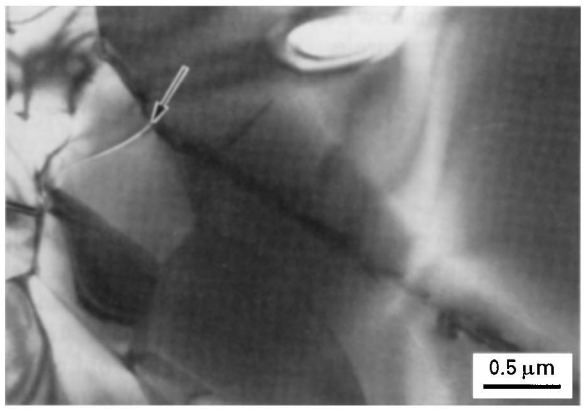


*Figure 7* Dislocation slip band (arrow) nucleating a transgranular microcrack in an adjacent grain.

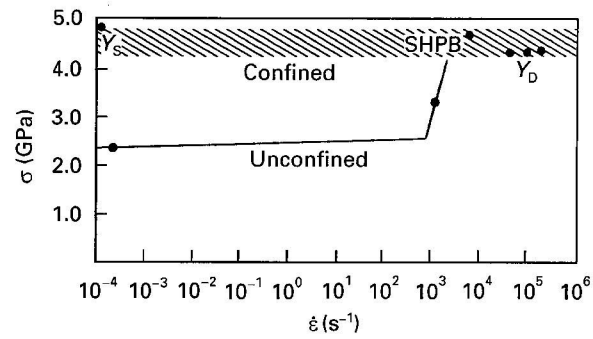


*Figure 8* Compressive yield strength for 99.5% $Al_2O_3$ derived from indentation hardness, $Y_S$, plate impact, $Y_D$, and confined SHPB experiments; strength is essentially strain-rate independent. Also shown are unconfined quasistatic and SHPB compression data, with strain-rate dependencies, based on crack kinetics, sketched in.

Typically, the former is defined as [14]

$$Y_S \simeq H/3 \tag{1}$$

while [16]

$$Y_D = 2\frac{c_s^2}{c_l^2}\,\mathrm{HEL} \tag{2}$$

where $c_s$ and $c_l$ are the shear and longitudinal sound speeds, respectively. For 99.5% $Al_2O_3$, $H = 14.5$ GPa, HEL = 10.6 GPa, $c_s = 6.24\,\mathrm{km\,s^{-1}}$, and $c_l = 10.56\,\mathrm{km\,s^{-1}}$ [16]. Based on these parameters and Equations 1 and 2, $Y_S \simeq 4.8$ GPa, and $Y_D = 4.3$ GPa. Grady has further shown [17] experimentally that over a limited dynamic strain-rate range, $Y_D$ is strain-rate independent.

The present experiments can be placed in perspective as shown in Fig. 8. Here the compressive yield strength of $Al_2O_3$ is given for a strain-rate range of $10^{-4}$–$10^{-6}\,\mathrm{s^{-1}}$, with the current confined high strain-rate experiment represented by the peak stress to which the sample was loaded beyond the hydrostate, i.e. 4.85 GPa. The results plotted in Fig. 8 lie within a tight range of stress levels, suggesting that the yield strength is virtually strain-rate insensitive.

Also shown are the unconfined data for quasistatic and dynamic (SHPB) compression. The curves drawn represent previously observed experimental behaviour. Under relatively slow loading conditions ($\dot{\varepsilon} = 1.5 \times 10^{-4}\,\mathrm{s^{-1}}$), compression strength is controlled by subcritical crack growth according to $\sigma_c \propto \dot{\varepsilon}^{1/1-n}$, where $n$ is the stress intensity–crack growth velocity exponent; for $Al_2O_3$, $n$ is approximately 50 [18]. At higher strain rates, strength is controlled by crack inertia, according to [19] $\sigma_c \propto \dot{\varepsilon}^{1/3}$. Intermediate confining states raise these curves [9], so that they eventually approach the strain-rate independent band shown in the figure.

Based on the TEM evidence and the shape of the stress–time history, it seems clear that the effect of the autofrettage confinement was to permit the sample to attain a stress level equal to the essentially strain-rate independent yield strength established by the microhardness and plate-impact experiments. It is known that extensive plastic flow is associated with $Al_2O_3$ hardness impressions [14], and Grady has recently hypothesized [20, 21] that it seems more reasonable to ascribe observed yielding within the shock front, i.e. the HEL, to plastic flow rather than to brittle microfracture. The present results appear virtually to assure that that is indeed the case. In particular, damage associated with the autofrettage experiment consisted of extensive dislocation arrays and slip bands, plus occasional microcracks nucleated by slip band pile-ups.

This is consistent with earlier work by Cagnoux and Longy [22] involving SEM and X-ray analysis of plate-impact fragments of 99.7% $Al_2O_3$, microstructurally similar to the present 99.5% $Al_2O_3$. Based on the absence of detectable microcracks, and the interpretation of X-ray line broadening, it was inferred that the shock ($\dot{\varepsilon} \simeq 10^5\,\mathrm{s^{-1}}$) stress regime from 0.9 HEL to 2.0 HEL is dominated by plastic flow.

The present work also appears to have implications regarding the nature of "conventional" compressive strength in ceramics. It has been noted [14] that there exist striking correlations between compressive strength and indentation hardness, at least in terms of trends, i.e. $\sigma_c \propto H$. Moreover, Lankford has shown [14] that when optimal compressive test conditions are utilized in conjunction with strong, near-theoretically dense (minimum porosity) ceramic bodies, there is obtained an almost 1:1 correlation between $Y_S$ and $\sigma_c$. This implies that under unconfined conditions, the highest compressive strength that can be attained is the intrinsic yield point, at which macroscopic plastic flow and associated microfracture will be inevitable, leading to rapid failure via microcrack coalescence. Under confinement, as demonstrated by Heard and Cline [8], this quasistatic limit can be exceeded, i.e. $\sigma_c > Y_S$, with monotonic hardening. The latter supports the interpretation of the present results (Fig. 3) that the confined sample under dynamic loading is experiencing stable post-yielding hardening.

## Acknowledgement

This work was performed under contract DAALO3-92-K-0001 with the US Army Research Office.

## Appendix.
## Analysis model for autofrettaged device

To achieve higher pressures, a steel confinement ring is shrink-fitted around the ceramic specimen. To maintain an elastic response in the confinement ring, the ring is actually composed of two concentric rings, with the outer ring shrink-fitted to the inner. This autofrettaged assembly is then shrink-fitted to the ceramic specimen, producing a compressive stress state in the specimen. During the shrink fitting, the ceramic is compressively loaded in order to achieve a hydrostatic state of stress.

To calculate the amount of axial loading required and determine the subsequent pressure on the ceramic specimen, the elastic equations with an assumed uniform strain in the axial direction were solved. In cylindrical coordinates, assuming no θ dependence, the strains are

$$\varepsilon_{rr} = \frac{\partial u_r}{\partial r}, \quad \varepsilon_{\theta\theta} = \frac{u_r}{r}, \quad \varepsilon_{zz} = \frac{\partial u_z}{\partial z}, \quad \varepsilon_{zr} = \frac{1}{2}\left(\frac{\partial u_z}{\partial r} + \frac{\partial u_r}{\partial z}\right) \tag{A1}$$

where $u_i$ represents the various displacements. Assuming that the axial displacement depends only upon $z$ and the radial displacement depends only upon $r$ yields $\varepsilon_{zr} = 0$. Given the strains, the stress state is obtained from Hooke's law

$$\sigma_{rr} = (\lambda + 2\mu)\frac{\partial u_r}{\partial r} + \lambda\frac{u_r}{r} + \lambda\varepsilon_{zz} - 3KA^T \tag{A2a}$$

$$\sigma_{\theta\theta} = \lambda\frac{\partial u_r}{\partial r} + (\lambda + 2\mu)\frac{u_r}{r} + \lambda\varepsilon_{zz} - 3KA^T \tag{A2b}$$

$$A^T = \int_{T_{room}}^{T} \alpha(T)\,dT$$

$$\sigma_{zz} = \lambda\frac{\partial u_r}{\partial r} + \lambda\frac{u_r}{r} + (\lambda + 2\mu)\varepsilon_{zz} - 3KA^T \tag{A2c}$$

where λ and μ are Lamé constants, and $A^T$ is the thermal expansion term. For the ceramic the coefficient of thermal expansion, α, is temperature dependent.

The equilibrium equation in cylindrical coordinates is

$$\frac{\partial\sigma_{rr}}{\partial r} + \frac{1}{r}(\sigma_{rr} - \sigma_{\theta\theta}) = 0 \tag{A3}$$

and when combined with Equations A2a–c it becomes

$$\frac{d}{dr}\left(\frac{1}{r}\frac{d}{dr}(ru_r)\right) = 0 \tag{A4}$$

The general solution, due to Lamé, is

$$u_r = Ar + \frac{B}{r} \tag{A5}$$

The resulting strains are

$$\varepsilon_{rr} = A - \frac{B}{r^2}, \quad \varepsilon_{\theta\theta} = A + \frac{B}{r^2} \tag{A6}$$

The stresses can now be written in terms of the known strains. The pressure is

$$P = -\frac{1}{3}\sigma_{ii} = -\frac{1}{3}\left[(3\lambda + 2\mu)\left(\frac{\partial u_r}{\partial r} + \frac{u_r}{r} + \varepsilon_{zz}\right) - 9KA^T\right]$$

$$= -K[2A + \varepsilon_{zz} - 3A^T] \tag{A7}$$

In order to estimate the confining pressure applied to the specimen from elastic considerations, the confinement sleeve cannot be allowed to yield, and to ensure that this is the case, the equivalent stress is compared with the yield stress of the steel confinement material. Therefore, to maintain an elastic condition, the pressure on the specimen is limited by the yield stress of the autofrettaged confining material. The equivalent stress is

$$\sigma_{eq} = (3J_2)^{1/2}$$

$$= \left\{\frac{1}{2}[(\sigma_{rr} - \sigma_{zz})^2 + (\sigma_{zz} - \sigma_{\theta\theta})^2 + (\sigma_{\theta\theta} - \sigma_{rr})^2]\right\}^{1/2}$$

$$= 2\mu[(A - \varepsilon_{zz})^2 + 3B^2/r^4]^{1/2} \tag{A8}$$

The equivalent stress is examined to see if the yield of the steel containment material is exceeded. The design is such that the maximum confining stress is actually limited by the temperature to which the autofrettaged ring can be raised, because for a wide range of temperatures the response is elastic.

The geometry is comprised of three regions, the inner ceramic specimen of radius $a$ and the two concentric steel rings for containment of outer radii $b$ and $c$. These regions will be indicated by the subscripts $I$, $II$, and $III$, respectively. In the inner region $B = 0$, because the solution must be well behaved at $r = 0$. A desired property in the inner region is that the stress state has no shear components, i.e. the load be purely hydrostatic, ($\sigma_{rr} = \sigma_{\theta\theta} = \sigma_{zz}$). This requires

$$A_I = \varepsilon_{zz} \tag{A9}$$

We assume that regions $II$ and $III$ are made of the same material so that, for example, $\lambda_{II} = \lambda_{III}$. The boundary conditions between the regions are defined below.

BC1: matching normal stresses ($\sigma_{rr}$) at $r = a$

$$3K_I(A_I - A_I^T) = 2(\lambda_{II} + \mu_{II})A_{II} - 2\mu_{II}\frac{B_{II}}{a^2}$$

$$+ \lambda_{II}(A_I + (\varepsilon_{zz})_0) - 3K_{II}A_{II}^T \tag{A10}$$

BC2: matching displacements at $r = a$

$$A_I a = A_{II} a + \frac{B_{II}}{a} \tag{A11}$$

BC3: matching normal stresses at $r = b$

$$2(A_{II} + \mu_{II})A_{II} - 2\mu_{II}\frac{B_{II}}{b^2} - 3K_{II}A_{II}^T$$

$$= 2(\lambda_{II} + \mu_{II})A_{III} - 2\mu_{II}\frac{B_{III}}{b^2} - 3K_{II}A_{III}^T \tag{A12}$$

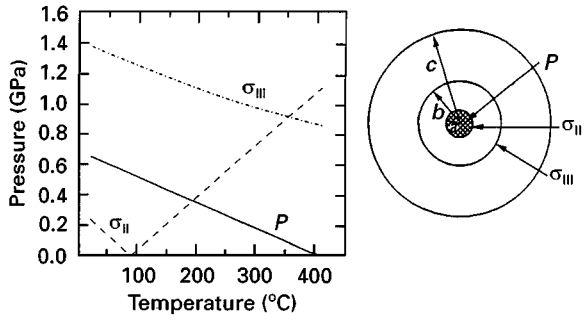


*Figure A1* Pressure and equivalent plastic strain as a function of temperature.

BC4: matching displacements at $r = b$

$$A_{II}b + \frac{B_{II}}{b} = A_{III}b + \frac{B_{III}}{b} \qquad \text{(A13)}$$

BC5: zero normal stress at outer surface

$$2(\lambda_{II} + \mu_{II})A_{III} - 2\mu_{II}\frac{B_{III}}{c^2} + \lambda_{II}(A_I + (\varepsilon_{zz})_0) - 3K_{II}A^T_{III} = 0 \qquad \text{(A14)}$$

These five boundary conditions provide a linear system of five equations in the five unknowns $A_I$, $A_{II}$, $B_{II}$, $A_{III}$, and $B_{III}$.

The above system is first solved with no specimen to determine the inner radius of the autofrettaged device upon heating to a given temperature. This provides a radius for the test specimen. To load the specimen, the autofrettaged steel confinement ring is heated and the room-temperature specimen is placed in the inner cavity. The specimen is axially loaded in compression while cooling occurs.

In the analytical solution, it is assumed there is no axial slip between the ceramic specimen and the inner steel confinement ring once the room-temperature specimen is inserted into the heated autofrettaged device. Thus, the axial displacement and strain, $\varepsilon_{zz}$, are the same for all regions. When the computation without the specimen is performed, an axial strain for just the autofrettaged ring is determined. This axial strain, $(\varepsilon_{zz})_0$, is used as an initial offset in the solution for the complete assembly. Use of this strain provides for the condition of no pressure on the specimen when it is initially inserted into the heated autofrettaged ring. After insertion, and as the temperature decreases, the axial strain is adjusted (through axial loading of the specimen) to maintain a hydrostatic state of stress within the sample. (Note that what is done to produce Fig. A1 is different from what is actually done in the test. For the former, gradual loading is applied during colling, while in the latter, the full load is applied initially and held while the specimen cools.) This then leads to a final pressure within the specimen at room temperature. It also allows evaluation of the equivalent stress at the inner surfaces of the steel rings, where it is greatest. For the specific geometry discussed below, Fig. A1 shows the values of the pressure in the room-temperature specimen and the maximum equivalent plastic stresses in each of the steel rings versus the temperature of the steel. It is seen, for high-strength steel with a yield strength of 2.4 GPa, that the stress state in the rings is well below yield.

## References


1. U. S. LINDHOLM, L. M. YEAKLEY and A. NAGY, *Int. J. Rock Mech. Min. Sci.* **11** (1974) 181.
2. R. ARROWOOD and J. LANKFORD, *J. Mater. Sci.* **22** (1987) 373.
3. S. SERDENGECTI and G. D. BOOZER, "Proceedings of the 4th Symposium on Rock Mechanics", Pennsylvania State University (1961) p. 83.
4. R. J. CHRISTENSEN, S. R. SWANSON and W. S. BROWN, *Exp. Mech.* **12** (1972) 508.
5. J. LANKFORD, C. E. ANDERSON Jr, G. R. JOHNSON and T. J. HOLMQUIST, in "Proceedings of the 1991 Combat Vehicle Survivability Conference", Vol. II, Gaithersburg, MD, 15–17 April (1991) pp. 67–73.
6. U. S. LINDHOLM, in "Techniques of Metals Research", Vol. 5(1), edited by R. F. Bunshah, (Wiley, New York, 1971), pp. 199–271.
7. C. E. ANDERSON, Jr, P. E. O'DONOGHUE, J. LANKFORD and J. D. WALKER, *Int. J. Fract.* **55** (1992) 193.
8. H. C. HEARD and C. F. CLINE, *J. Mater. Sci.* **15** (1980) 1889.
9. W. CHEN and G. RAVICHANDRAN, *J. Am. Ceram. Soc.* **79** (1996) 579.
10. J. D. WALKER, A. NAGY, C. E. ANDERSON Jr, J. LANKFORD and A. E. NICHOLLS, in "Materials Application of Shock Waves and High-Strain-Rate Phenomena", edited by L. E. Murr, (Elsevier Science, B.V.) in press.
11. C. E. ANDERSON Jr, J. D. WALKER and J. LANKFORD, "Investigations of the ballistic response of brittle materials", SwRI Report 06-5117/002, US Army Research Office, Research Triangle Park, NC 27709 (1995).
12. J. M. STAEHLER, W. W. PREDEBON, B. J. PLETKA and J. LANKFORD, *J. Am. Ceram. Soc.* **76** (1993) 536.
13. G. RAVICHANDRAN and G. SUBHASH, *ibid.* **77** (1994) 263.
14. J. LANKFORD, *J. Hard Mater.* **2** (1991) 55.
15. D. E. GRADY, "Dynamic material properties of armor ceramics", Sandia Report no. SAND91-0147, Sandia National Laboratories, Albuquerque, NM, March 1991.
16. D. E. GRADY and J. L. WISE, "Dynamic properties of ceramic materials", Sandia Report no. SAND93-0610, Sandia National Laboratories, Albuquerque, NM, September 1993.
17. D. E. GRADY, in CIMNE, Barcelona, 1995, to be published.
18. J. LANKFORD, *J. Am. Ceram. Soc.* **64** (1981) C-33.
19. M. E. KIPP, D. E. GRADY and E. P. CHEN, *Int. J. Fract.* **16** (1980) 471.
20. D. E. GRADY, "Dynamic properties of ceramic materials", Sandia Report no. SAND94-3266, Sandia National Laboratories, Albuquerque, NM, February 1995.
21. *Idem*, in "1995 APS Topical Conference on Shock Compression of Condensed Matter", Seattle, WA, 13–18 August 1995.
22. J. CAGNOUX and F. LONGY, *J. Phys.* **49** (1988) C3.3.


*Received 27 August*
*and accepted 30 October 1996*